Serine Phosphorylation Regulates the P-type Potassium pump KdpFABC

Marie E. Sweet[1], Vikas Dubey[2], Xihui Zhang[1], Hediye Erdjument-Bromage[1], Thomas A. Neubert[1], Bjørn P. Pedersen[3], Himanshu Khandelia[2], David L. Stokes[1]

[1] Skirball Institute, Dept. of Cell Biology, New York University School of Medicine, New York, NY 10016 USA

[2] Dept. of Physics, Chemistry and Pharmacy, University of Southern Denmark, DK-5230 Odense M, Denmark

[3] Dept. of Molecular Biology and Genetics, Aarhus University, 8000 Aarhus-C, Denmark

Abstract

KdpFABC is an ATP-dependent K^+ pump that ensures bacterial survival in K^+-deficient environments. Whereas transcriptional regulation of kdpFABC expression is well studied, a mechanism for regulating the pump when K^+ levels are restored has not been described. Here we show that KdpFABC is inhibited by serine phosphorylation when cells return to a K^+-rich environment. The mechanism of inhibition involves phosphorylation of Ser162 on KdpB, which is reversed by serine phosphatase. Mutating Ser162 to Alanine produces constitutive activity, whereas the phosphomimetic Ser162Asp mutation inactivates the pump. Analyses of partial reactions in the transport cycle show that serine phosphorylation uncouples the pump and blocks the cycle after formation of the catalytic aspartyl phosphate intermediate (E1~P). Molecular dynamics simulations show that serine phosphorylation affects domain dynamics that explain the uncoupling. This regulatory mechanism, unique amongst P-type pumps, furthers our understanding of how bacteria control potassium homeostasis to maintain cell volume and osmotic potential.

Introduction

Potassium is the primary osmolyte used by cells to maintain homeostasis and facilitate cell growth. A sizeable difference in K^+ concentration across the plasma membrane is largely responsible for setting the membrane potential, is essential for regulating intracellular pH, for generating turgor pressure required for cell growth and division and as an energy source for diverse transport processes (Altendorf et al., 2009; Epstein, 2003). When external K^+ concentrations are in the millimolar range, Trk and Kup are two constitutively expressed K^+ uptake systems that are sufficient to maintain K^+ homeostasis of bacteria. However, when extracellular K^+ concentrations fall into the micromolar range, a high-affinity, active transport system called Kdp takes over. The kdp genes, which underlie the only inducible K^+ transport system in bacteria, are organized into two adjacent operons (kdpFABC and kdpDE). The latter is responsible for sensing the environment and controlling the expression of kdpFABC (Jung and Altendorf, 2002). The KdpFABC protein complex is an ATP-dependent K^+ pump that has micromolar affinity for K^+ and is capable of generating a gradient up to six orders of magnitude, thus maintaining intracellular concentrations between 0.1 and 1M even when extracellular K^+ is present in trace amounts (Ballal et al., 2007).

Although the mechanisms for activating transport by KdpFABC have been studied in considerable detail, the field has largely overlooked the need to suppress the pump once external K^+ levels return to the millimolar range. On the one hand, it is clear that activation of transport is done at the transcriptional level via KdpD/E, a two-component system in which KdpD serves as the sensor kinase and KdpE as the response regulator (Walderhaug et al., 1992). When the cell's need for K^+ is not being met, KdpD phosphorylates and thus activates KdpE, which then induces expression of the KdpFABC pump (Jung et al., 2012). The signal acting on KdpD is still controversial, with recent studies favoring external K^+ concentration (Laermann et al., 2013), internal Na^+ or NH_4^+ concentrations (Epstein, 2015) or dual binding sites for K^+ that sense the gradient across the membrane (Schramke et al., 2016). On the other hand, inhibition of transport by KdpFABC has been observed when cells are returned to K^+-rich media (Rhoads et al., 1978; Roe et al., 2000). Although the mechanism is unknown, inhibition of transport under these conditions is necessary to prevent wasteful usage of ATP and a skyrocketing of the intracellular K^+ concentration. Transcriptional repression is an unlikely explanation because the inhibitory effect is rapid (<2 min in K^+ rich media) compared to the much slower rate of protein turnover in bacteria (Trotschel et al., 2013). Indeed, the authors reporting this effect suggested that existing KdpFABC molecules may be directly inhibited by some unreported mechanism (Roe et al., 2000).

Recent structural analysis revealed phosphorylation of a serine residue in a cytoplasmic domain of the KdpB subunit within a highly conserved TGES sequence motif (Huang et al., 2017). This observation was surprising, given the prominence of the $TGES^{162}$ motif in the catalytic cycle of related P-type ATPases and the lack of precedent for an analogous post-translational modification in this well-studied superfamily of ATP-dependent cation pumps (Palmgren and Nissen, 2011). P-type ATPases including KdpB share a reaction cycle known as the Post-Albers scheme (Fig 1a) that begins with formation of an aspartyl phosphate on a conserved sequence ($D^{307}KTGT$) in the centrally located cytoplasmic domain (P-domain). This transient phosphoenzyme intermediate (E1~P) serves to harness the energy of ATP and then to drive conformational changes that lead to ion transport. The highly conserved TGES motif is found in a second cytoplasmic domain (A-domain) with the glutamate residue playing a crucial role in hydrolysis of the aspartyl phosphate in the second half of the catalytic cycle (E2-P -> E2) (Moller et al., 2010). An X-ray structure of KdpFABC showed that the serine adjacent to this catalytic glutamate residue carried a phosphate moiety and that this moiety interacted with positively charged residues on the third cytoplasmic domain (N-domain) (Huang et al., 2017). The ability of a protein phosphatase to increase ATPase activity supported the idea that serine phosphorylation induced an inhibited conformation perhaps stabilized by the crystal lattice. Phosphorylation of Ser162 was also seen in subsequent cryo-EM structures from another group (Stock et al., 2018), although this work revealed different conformations that disrupted the interaction between A- and N-domains.

To further explore the inhibitory effects of serine phosphorylation, we have established growth conditions that lead to phosphorylation of Ser162 on KdpB and have characterized its effect on individual steps in the reaction cycle. Consistent with previous observations (Roe et al., 2000), we found that moving cells to K^+-rich media resulted in an inhibition of KdpFABC in a time-dependent manner. We found that KdpFABC activity was inversely proportional to the extent of serine phosphorylation and that activity was proportionately restored by removing the phosphate with lambda protein phosphatase (LPP). To elucidate the mechanism of inhibition, we measured steady-state levels of the aspartyl phosphate intermediates (EP). We found that

the KdpB-S162A mutation, which prevented serine phosphorylation, produced much lower steady-state levels of EP and that a phosphomimetic mutation, KdpB-S162D, mimicked the inhibitory effect of serine phosphorylation. Although steady-state levels of EP for the fully active KdpB-S162A mutant was K^+-dependent, phosphorylation or the phosphomimetic S162D mutation eliminated this K^+-dependence. Pulse chase studies with ADP indicated that serine phosphorylation trapped the pump in the E1~P state. Molecular dynamics simulations were used to characterize the dynamics of the protein. These simulations showed that, when Ser162 was phosphorylated, there was a dramatic increase in mobility of the cytoplasmic domains and that an aqueous channel opened and hydrated a functional site in the transmembrane domain of KdpB where P-type ATPases typically bind cations. We conclude that the serine phosphorylation signal is propagated via the cytoplasmic domains to the transmembrane site via an allosteric network, thus perturbing the pumping cycle and leading to the observed inhibition.

RESULTS

Survey of KdpFABC mutants reveals unexpected inhibition

An overarching goal of our work is to understand the allosteric coupling between KdpA and KdpB that gives rise to ATP-dependent K^+ transport. To this end, we setup a survey of alanine substitution mutants to evaluate the role of various residues implicated by the X-ray crystal structure (Suppl. Table 1). For expression of these mutants, plasmids carrying a His-tagged version of the kdpFABC operon under control of the native promoter were transformed into E. coli strain TK2498 (Suppl. Table 2) and cells were grown in media with limiting K^+ concentrations (0.2 mM) in order to induce expression. Although this strain lacks constitutive K^+ transport systems (Trk and Kup), it has a chromosomal copy of kdpFABC-Q116R, which is a low K^+ affinity mutant that ensured cell survival even when the expression plasmid encoded a dysfunctional Kdp mutant. The purification protocol used to isolate the mutant KdpFABC proteins excluded this chromosomal copy because it lacked a His-tag. Unexpectedly, the ATPase activities of all of the mutants were very low (Fig. 1b), causing us to explore unanticipated parameters that might have influenced these measurements. Based on our earlier evidence that phosphorylation of Ser162 in KdpB is inhibitory (Huang et al., 2017), we used mass spectrometry to determine levels of this post-translational modification (Suppl. Fig. S1), which were all extremely high (Fig. 1c). The inhibitory effect of Ser162 phosphorylation was supported by the effects of LPP, which produced significant stimulation in ATPase activity when applied to several of the preparations (Fig. 1d). WT protein and the D307A mutation in KdpB served as positive and negative controls, respectively. As expected, the D307A mutant was catalytically inactive because this residue is the site of aspartyl phosphate (E1~P) formation. It is notable that the WT construct had virtually no serine phosphorylation. Given the high affinity of WT protein for K^+, it was expressed at 50-100x lower levels of K^+ (<10 μM) in the TK2499 strain that lacks other copies of the kdpFABC gene. We therefore set out to determine whether phosphorylation of Ser162, and consequent inhibition of KdpFABC, was a cellular response to elevated K^+ in the media.

Increased K^+ is a physiological stimulus for serine phosphorylation

To test whether elevated K^+ concentrations lead to serine phosphorylation, we first grew cells with WT KdpFABC under K^+ limiting conditions and then split the culture into two batches immediately prior to harvest. To one batch we added 20 mM K^+ - so called K^+ shock - and growth was allowed to continue for 20 min. KdpFABC was then purified from both batches.

ATPase assays documented a 40% inhibition for protein derived from the cells subjected to the K^+ shock, which was fully restored after treatment with LPP (Fig. 2a). Mass spectrometry confirmed a higher level of serine phosphorylation for the protein derived from the K^+ shock, estimated to be 27% vs 1% for the control based on peptide ion intensities for phosphorylated and nonphosphorylated peptides. These percentages are nominal because phosphorylated and nonphosphorylated versions of the same peptide are not ionized and detected with equal efficiency and, as a result, positive ion mass spectrometry typically underestimates the level of phosphorylation (Xu et al., 2005). However, relative phosphorylation levels of different samples are reliable (Huang et al., 2016) and these data show that the K^+ shock resulted in phosphorylation of Ser162 as well as inhibition of ATPase activity.

Time dependence of serine phosphorylation

To extend these studies, we varied the length of time that cells were subjected to the K^+ shock in order to characterize the time dependence of the response. For each experiment, the culture was split, 20 mM added to one half and incubated for either 0, 10, or 90 min before harvesting the cells. The incubation time is nominal given that cells were exposed to the media during the 20 min centrifugation step. ATPase inhibition increased as incubation time increased (15%, 25%, and 74%) and LPP treatment largely relieved this inhibition (Fig. 2c). In addition to mass spectrometry, we used SDS-PAGE together with Phos-tag stain (Suppl. Fig. S2) to quantify levels of serine phosphorylation. Results from mass spectrometric phosphorylation analysis were consistent with this graded response to the K^+ shock (increases of 2.07, 4.02 and 5.23 fold, respectively) and confirmed Ser162 as the site of phosphorylation (Suppl. Fig. S1). However, data from Phos-tag staining was more consistent across samples and these data clearly illustrate a time-dependent increase in serine phosphorylation that accompanied the loss of ATPase activity (Fig. 2d).

In addition to these isolated experiments, we conducted a time course in which a single culture was split into four batches that were treated for varying times with 20 mM K^+. In addition to a control, untreated batch, the cultures were exposed to K^+ shock conditions for 0, 20 and 60 min prior to harvesting the cells. ATPase activities of the corresponding preparations of KdpFABC show an increasing amount of inhibition, which was largely reversed by treatment with LPP (Fig. 2e), and increasing levels of serine phosphorylation (Fig. 2f). Aggregation of data from all of these experiments showed a clear correlation between ATPase activity and serine phosphorylation for both mass spectrometry (Fig. 2g) and Phos-tag staining (Fig. 2h). Data from the two alternative approaches were also highly correlated (Fig. 2i). The intercept on the x-axis represents an estimate for ATPase activity of the uninhibited pump, which is similar for the two approaches (12.4 and 11.0 μmoles/mg/min respectively). The intercept on the y-axis allows scaling of the level of serine phosphorylation, which is shown on the right-hand axis and suggests an ion intensity scaling factor of ~2.5 for percentages determined by mass spectrometry. Combining the site specificity of mass spectrometry with the quantification accuracy of Phos-tag staining, we conclude that a return to K^+-rich media causes phosphorylation of Ser162 with a concomitant and proportional inhibition of ATPase activity.

Substrate affinities and energy coupling are not affected by serine phosphorylation

To investigate how serine phosphorylation inhibits turnover of KdpFABC, we used ATPase activity to estimate substrate affinities. In principle, a lower affinity for either K^+ or ATP might account for the observed reduction in ATPase activity. For measuring K^+ and ATP affinities we used the KdpA-Q116R mutant, which was previously denoted kdp-42 or strain

TK2242-42 in the literature (Epstein et al., 1978; Siebers and Altendorf, 1989). The well documented reduction in K^+ affinity for this mutant to the millimolar range (Buurman et al., 1995) makes it practical to titrate K^+ concentration during activity assays. This mutant was expressed at high K^+ concentrations using the pBAD promoter, thus producing high levels of serine phosphorylation that were evident from an ~4-fold stimulation from LPP treatment (V_{max} = 1.2 and 5.0 μmoles/mg/min in Fig. 3a). Titration curves from untreated and treated samples indicated that K_M for K^+ (8.6 mM and 10.9 mM, respectively) and ATP (123 μM and 118 μM) were not significantly affected by serine phosphorylation (Fig. 3a,b). In addition, we tested inhibition by orthovanadate, which acts as a transition state analogue for inorganic phosphate and binds to the E2 state to form an inhibitory complex (Clausen et al., 2016). The IC_{50} for orthovanadate reflects not only an intrinsic binding affinity but also the conformational equilibrium between E2 and E1 states of P-type ATPases (Toustrup-Jensen et al., 2001). For measuring orthovanadate inhibition we used WT KdpFABC before and after K^+ shock, which produced an ~2-fold reduction in ATPase activity (Fig. 3c). Comparison of these samples under standard ATPase conditions (150 mM K^+ and 2.4 mM ATP) indicate no significant change in IC_{50} (29.86 μM vs. 34.75 μM), indicating that serine phosphorylation also does not affect the E1/E2 conformational equilibrium.

To test whether serine phosphorylation affected coupling of ATPase activity to K^+ transport, we reconstituted KdpFABC into proteoliposomes and measured transport. As in previous work (Fendler et al., 1996), a voltage-sensitive dye (DiSC3) was used to report electrogenic transport of K^+ into the vesicles. Upon addition of ATP, a robust decrease in fluorescence reported on the buildup of a positive membrane potential (Suppl. Fig. S3). The initial part of the curve was fitted with an exponential to quantify the rate (Damnjanovic and Apell, 2014a) and to compare the preparation before and after LPP treatment. This analysis shows an excellent correlation between ATPase activity and transport indicating that serine phosphorylation also does not affect the coupling of the pump.

Effect of serine phosphorylation on partial reactions

Formation of an aspartyl phosphate at the catalytic site in the P-domain is a key step in the reaction cycle (Fig. 1a). To evaluate how serine phosphorylation affects the formation of the high-energy phosphoenzyme (E1~P), as well as the following spontaneous conversion to the low-energy phosphoenzyme (E2-P), we used a conventional assay employing [γ^{32}P]-ATP to initiate the reaction followed by an acid quench at defined time intervals. This assay reports on steady-state levels of aspartyl phosphorylation (EP), which includes molecules in both E1~P or E2-P. These two states were then distinguished by their reactivity to ADP, based on the fact that E1~P is readily dephosphorylated by ADP but E2-P is not (Toustrup-Jensen et al., 2001). We conducted experiments in the presence and absence of K^+ to elucidate the causality between ion binding and EP formation, which is currently unclear (Pedersen et al., 2019). For this analysis, we used the KdpA-Q116R mutation with its lower K^+ affinity. We also used the KdpB-S162A mutation to prevent serine phosphorylation and the KdpB-S162D mutation as a phosphomimetic, both on the KdpA-Q116R background. For a negative control, we mutated the catalytic Asp307 residue in KdpB, which completely prevents phosphoenzyme formation. For a positive control we introduced the KdpB-E161Q mutation which typically blocks hydrolysis of the E2-P species. Both of these controls included the KdpA-Q116R mutation and the E161Q construct also carried the KdpB-S162A mutation to prevent serine phosphorylation (see summary of constructs in Suppl. Table 1). All relevant constructs were expressed in E. coli

using a pBAD promoter in K^+ rich media which activated the pathway for serine phosphorylation, which is evident from the 3-4 fold stimulation in ATPase activities after LPP treatment (Figs. 3a & b and Suppl. Fig. S2). The KdpB-D307A, KdpB-E161Q and KdpB-S162D mutations all resulted in complete inhibition of ATPase activity even after LPP treatment.

Typical experiments are shown in Figs. 4a and b, which represent the time course of EP formation in the absence and presence of 10 mM K^+ respectively. In the presence of K^+, EP levels of active constructs (i.e., Q116R and S162A) decay over time as the ATP in the solution is exhausted (Fig. 4b). In contrast, EP levels were stable in the absence of K^+, because there is no enzymatic turnover (Fig. 4a), and at 4°C, because of a much slower turnover rate (data not shown). EP levels were also stable for inactive constructs (i.e., S162D and E161Q). Data from 15 individual experiments have been normalized and pooled in Fig. 4c. These data included all points for experiments with low turnover rates (i.e., 4°C or lacking K^+) and initial points for experiments with high turnover rates (i.e., room temperature in the presence of K^+) or pulse chase (see below). Normalization of data from each experiment was based on data from KdpB-E161Q, which consistently produced the highest levels of EP and which were stable over the course of the experiment. Thus, data in Fig. 4c indicate that Q116R and S162D constructs, which both reflect the effects of Ser162 phosphorylation, produced high levels of EP both in the presence and absence of K^+. In contrast, EP levels for the Ser162A construct, which cannot be serine phosphorylated, are much lower and showed a significant dependence on K^+. As expected, the D307A construct produced negligible levels of EP. These data suggest that the first step of the reaction cycle - formation of the aspartyl phosphate - is K^+-dependent and that phosphorylation of Ser162 not only uncouples this step but also prevents the hydrolysis of the phosphoenzyme intermediate.

In order to determine more precisely where the cycle was blocked by serine phosphorylation, we used a pulse-chase strategy to distinguish E1~P from E2-P intermediates. For this assay, we initiated phosphoenzyme formation in the presence of K^+ with [γ^{32}P]-ATP at 4°C where steady-state levels are stable. After 15 sec, an aliquot was removed (plotted as time zero) and a solution containing 10 mM ADP and 10 mM EDTA was added to determine the proportion of E1~P present. Fig. 4d shows that EP levels for KdpB-S162A and KdpB-S162D are immediately reduced to zero. This result indicates that E1~P is the prevalent species at steady state and that serine phosphorylation prevents the molecule from progressing to the E2-P state. The KdpB-E161Q construct (which also included KdpA-Q116R and KdpB-S162A mutations) is known to trap the E2-P state and, as expected, is completely unreactive with ADP.

Effects of serine phosphorylation on structural dynamics

We have used MD simulations to study the effects of serine phosphorylation on the structural dynamics of KdpFABC. For these simulations, we started with the crystal structure (PDB code 5MRW) and placed it in a system with explicit solvent consisting of a membrane bilayer composed of 80% 1-palmitoyl-2-oleoyl-sn-glycero-3-ethanolamine and 20% 1-palmitoyl-2-oleoyl-sn-glycero-3-phosphoglycerol and an aqueous compartment composed of water and 150 mM KCl. After equilibrating this system, ten independent simulations of 200 ns were launched for KdpFABC with and without serine phosphorylation, referred to as PHOS and SER simulations respectively. The simulations revealed distinct and reproducible differences in the behavior of KdpB that we attribute to serine phosphorylation. The first difference involved the canonical ion-binding site of P-type ATPases formed near Pro264 on the M4 helix. This site is occupied by a water molecule in the crystal structure of KdpB (Fig. 5b) and, in the PHOS

simulations, this water molecule escaped almost immediately, whereas it remained bound for the duration of the SER simulations. This escape was facilitated by the opening of an aqueous channel in KdpB from the cytoplasmic side of the membrane (Fig. 5c). In contrast, water did not reach the canonical ion-binding site and the initial water molecule remained occluded in the SER simulations. (Fig. 5d). To quantify the penetration of water into this site, the radial distribution function (g(r)) was calculated for all water molecules relative to the center of mass defined by Pro264, Thr265, Asp583, and Lys586, which surround the site and coordinate the water molecule in the crystal structure (Fig. 5a). These data indicate that this canonical ion-binding site becomes highly hydrated when Ser162 on KdpB is phosphorylated, but not for the unphosphorylated Kdp complex.

The second difference caused by serine phosphorylation involved the mobility of the cytoplasmic domains of KdpB. In particular, the average deviations of each cytoplasmic domain relative to their starting positions were significantly higher in PHOS simulations, which can be seen in the RMSD distributions for the individual domains (Figure 6). In the crystal structure, the phosphate moiety on Ser162 as well as the neighboring Glu161 residue in the A-domain mediate salt bridge interactions with basic residues in the N-domain (Arg363 and Lys357, Suppl. Fig. S4). Despite the increase in overall movement in cytoplasmic domains of PHOS simulations, this salt bridge was relatively stable, as illustrated by the sharp radial distribution functions relating these residues (Suppl. Fig. S4a,b). In contrast, the radial distribution functions for SER simulations are broad, indicating that the A- and N-domains became rapidly uncoupled in the absence of serine phosphorylation.

A covariance and principal components analysis further elucidates the differing dynamic behaviors in PHOS and SER simulations. The first two eigenvectors of the covariance matrix representing atomic fluctuations account for the largest deviations in the dataset (Suppl. Fig. S5) and were used to analyze the global collective motions. For this analysis, each protein conformation sampled during the simulations was projected upon the two dimensional space formed by the first two eigenvectors (Fig. 7a). This projection map reveals several clouds which correspond to distinct protein conformations sampled during the simulations. These clouds are likely to represent free energy minima in the protein conformational landscape and this analysis reveals novel conformations, labeled C and D, that are sampled only in the PHOS simulations. In contrast, the molecules in the SER simulations remain within the larger cloud of conformations labeled B. A *k*-means clustering algorithm was used to extract representative structures from each conformational cluster, which are illustrated in Figs. 7B, 7C and 7D. In conformations C and D, sampled only in the PHOS simulations, the A-domain (yellow) uncouples from the P-domain (blue), and collapses towards the membrane. A similar uncoupling is observed for the N-domain (red) domain, which nevertheless remains tethered to the A-domain via the phosphorylated TGES motif.

These combined differences in cytoplasmic domain movements and hydration of the canonical ion-binding site in KdpB indicates that serine phosphorylation in the A-domain influences the behavior of the membrane domain. The coupling of these domains across a distance of almost 50 Å implies the existence of a long-range allosteric network. A closer examination of the structural elements connecting the A-domain with the membrane reveals a potential interaction between residues Glu87 and Arg212 at the cytoplasmic ends of M2 and M3, respectively (Fig 8a). The movement of the A-domain in the PHOS simulations is associated with an unfolding of the linker between M2 and the A-domain and a displacement of

these residues (Fig 8b-d), thus opening up the water pathway leading to the canonical ion-binding site near Pro264. This observation suggests that this region of KdpB provides a network of interactions for transmitting allosteric signals and that phosphorylation of Ser162 engages this network to prematurely hydrate the canonical cation binding site.

DISCUSSION

Our work has shown that phosphorylation of Ser162 on KdpB inhibits both ATPase and K^+ transport activity of KdpFABC without affecting substrate affinities or energy coupling. We have also documented that this posttranslational modification is a physiological response to elevated K^+ concentrations in the growth media. Specifically, whereas kdpFABC expression is induced by K^+ deficient media, a return to K^+ rich media gives rise to serine phosphorylation and inhibition of transport. This response explains earlier studies in which cell-based K^+ uptake by KdpFABC was irreversibly inactivated under similar conditions (Rhoads et al., 1978; Roe et al., 2000). The work by Roe et al. (Roe et al., 2000) also showed that the inhibition was irreversible, that the effect was specific to K^+ and was not due to osmotic upshock, which in any case would be very modest with the addition of only 20 mM KCl. Although these authors showed complete inhibition in cell based assays of transport, we achieved only ~75% maximal inhibition of purified protein after much longer incubation times in K^+ rich media (90 min vs 2 min). This difference might be explained by the much higher expression levels used for the current study, which employed a multicopy plasmid designed to produce high levels of protein expression suitable for biochemical purification compared to a single chromosomal copy used for previous work. The higher expression level might affect the extent of the phosphorylation either by exceeding the capacity of the (still unknown) kinase system or by changing the ionic balance of cells and thus influencing the sensing mechanism. The trigger could be complex as illustrated by the KdpD/E system which does not respond to a simple threshold concentration, but senses the "need" for K^+ by comparing intracellular and extracellular environments (Schramke et al., 2016).

P-type ATPases are subject to a variety of regulatory strategies, but the inhibition of KdpFABC by phosphorylation of the TGES motif represents a novel approach for this superfamily. In the case of plasma-membrane Ca^{2+}-ATPase (PMCA) (Cali et al., 2017), yeast and plant H^+-ATPases (Haruta et al., 2015), and the yeast lipid flippase (Drs2p) (Jacquot et al., 2012), the pumps are held in autoinhibited states by C-terminal domains. Similarly, phospholamban (PLB) and sarcolipin (SLN) are regulatory subunits that inhibit Ca^{2+}-ATPase from sarcoplasmic reticulum (SERCA) (Primeau et al., 2018) and FxYD proteins regulate Na/K-ATPase (Garty and Karlish, 2005). In most cases, these regulatory domains/subunits interact with the conserved catalytic domains to prevent turnover; distinct physiological factors bind to or modify these regulatory domains/subunits to disrupt these interactions and allow catalytic domains to function. These stimulatory factors are diverse and include Ca^{2+}/calmodulin for PMCA, phosphatidylinositol-4-phosphate for Drs2p and serine phosphorylation for the others. The regulatory mechanism for KdpFABC is novel in that the modification inhibits rather than stimulates the transport cycle and that the modification is applied directly to one of the catalytic domains rather than to an accessory structural element.

Although serine phosphorylation is well-known in eukaryotes, there are relatively few examples in bacteria. More commonly, signaling cascades in bacteria involve phosphorylation of histidine or aspartate residues, typically involving two-component systems such as KdpD/E.

Correspondingly, few Ser/Thr kinases have been identified in bacteria. In fact, a catalogue of bacterial signal transduction systems lists only two eukaryotic-like Ser/Thr kinases in E.coli: ubiB and yegI (Galperin et al., 2010). The former is involved in the ubiquitin biosynthesis pathway (Poon et al., 2000), whereas the latter has been characterized *in vitro* but has no known function *in vivo* (Rajagopalan et al., 2018). These Ser/Thr kinases are thought to have originated in eukaryotes and their presence in bacteria to be the result of horizontal gene transfer (Lai et al., 2016). If so, it would seem unlikely that a process as fundamental as osmotic homeostasis would be acquired by this mechanism. Atypical Ser/Thr kinases have also been reported in prokaryotes, such as the Hpr kinase that controls metabolism of carbon sources in gram positive bacteria, SpoIIAB, RsbT and RsbW that act on sigma factors to control sporulation and stress response in B. subtilis (Pereira et al., 2011), and AceK in E. coli that phosphorylates isocitrate dehydrogenase to control metabolism through the TCA cycle (Cortay et al., 1988). Their involvement in regulation of KdpFABC is worth considering. An intriguing alternative is that KdpB engages in autophosphorylation; if so, it must be very inefficient or require special conditions, because self-inhibition did not occur over the time course of our ATPase assays, nor has it been reported in the literature. The possibility that phosphate is transferred from Asp307 to Ser162, is inconsistent with the high levels of phosphorylation observed on the KdpB-D307A mutant (Fig. 1c). Another possibility is that phosphate is transferred directly from ATP to Ser162, but the complete lack of signal in EP formation experiments using the D307A mutation (Fig. 4) does not support this idea. Another intriguing possibility is that KdpD, which is already designed to sense the K^+ need of the cell (Schramke et al., 2016), would regulate activity of a Ser/Thr kinase that targets KdpFABC, as has been seen in several other systems (Pereira et al., 2011), but this scenario will require further investigation.

The correlation of serine phosphorylation with cell growth conditions and its inhibitory effects has important ramifications for our understanding of the reaction cycle of KdpFABC. Earlier work has concluded that formation of E1~P was K^+-independent, that K^+ bound to the E2-P state and was transported across the membrane during hydrolysis of the aspartyl phosphate (Damnjanovic and Apell, 2014b; Siebers and Altendorf, 1989). According to this scheme, K^+ transport by KdpFABC is analogous to K^+ transport by Na^+/K^+-ATPase (Goldshleger et al., 2001) or lipid by lipid flippases (Jacquot et al., 2012). However, this conclusion is at odds with recent structural work in which KdpB adopted an E1-like structural state when K^+ was bound in the selectivity filter of KdpA (Huang et al., 2017; Stock et al., 2018). In the current work, we also observed high levels of EP formation in the absence of K^+ as reported in earlier work, but only when KdpB was serine phosphorylated or carried the S162D mutation to mimic serine phosphorylation. In contrast, when the S162A mutation was used to prevent this phosphorylation, we observed much lower levels of EP formation and a clear dependence on the presence of K^+. The lower levels of EP in the presence of K^+ likely reflects rapid turnover by the S162A construct which therefore spend a lower fraction of time in one of the phosphoenzyme states (E1~P or E2-P). Inactive constructs, such as S162D, E161Q, and the serine phosphorylated species are essentially stuck in one of these phosphoenzyme states. ADP-sensitivity seen in the pulse chase experiments show that E1~P is the prevalent species and that serine phosphorylation prevents the E1~P to E2-P transition. In contrast, the E161Q mutation is known to prevent hydrolysis of the aspartyl phosphate {Clausen, 2004 #2555}), thus preventing the E2-P to E2 transition and, as expected, the phosphoenzyme formed by this construct does not react with ADP. We conclude, therefore, that formation of E1~P by functional KdpFABC molecules is dependent on K^+ binding and that K^+ is likely transported across the

membrane during the transition to the E2-P state, analogous to Na^+ transport by Na^+/K^+-ATPase.

MD simulations suggest allosteric communication from Ser162 in the A-domain to the canonical cation-binding site for P-type ATPases which contribute to the effects of serine phosphorylation. Like other P-type ATPases, the N- and A-domains of KdpB are highly mobile and are expected to adopt different configurations as the molecule moves through the reaction cycle (Moller et al., 2010). Indeed, these domains are disordered in the cryo-EM structure of the E1 state and there are dramatic differences in domain orientations in the X-ray structure, representing an inhibited E1 state, compared to the cryo-EM structure of the E2-P state (Huang et al., 2017; Stock et al., 2018). The MD simulations showed that serine phosphorylation enhanced these domain movements and that the effects were propagated across KdpB to open an aqueous channel leading to the canonical cation-binding site next to the M4 helix and Pro264. This aqueous channel provides a plausible explanation for the loss of K^+ dependence in EP formation. Specifically, once the channel is opened, cations from the aqueous milieu would be able to reach this canonical cation-binding site, thus bypassing the selectivity mechanism and coupling with KdpA. In analogy with other P-type ATPases, cation binding to this canonical site in KdpB would be expected to stimulate formation of the aspartyl phosphate. A role for M1 and M2 in controlling access to this site is consistent with their roles in controlling access of substrate in the case of SERCA (Sorensen et al., 2004) and lipid flippases (Hiraizumi et al., 2019). However, the cytosolic channel observed in our MD simulations differs from the 'exit pathway' described by Stock et al. (Stock et al., 2018), which emerges near the interface between KdpA and KdpB.

The structures of KdpFABC feature a unique intramembrane tunnel that runs between the selectivity filter of KdpA and the canonical cation-binding site in KdpB. There are currently two models for transport of K^+ across the membrane, which differ in the role played by this tunnel. In the first (Huang et al., 2017), the tunnel is filled with water; when K^+ enters the selectivity filter, a positive charge propagates through the tunnel and protonates a water molecule bound at the canonical site in KdpB, thus initiating E1~P formation. K^+ is then transported through KdpA in the latter half of the reaction cycle. In the second (Stock et al., 2018), K^+ actually moves through the tunnel and occupies the canonical cation site to initiate E1~P formation. K^+ could then be released to the cytoplasm via one of the aqueous channels. The current work cannot distinguish between these two models, but does strongly suggest that efforts should be made to ensure that serine phosphorylation is not a factor in future structural and biochemical work on KdpFABC.

Acknowledgements

We thank Jingjing Deng for initial mass spectrometry analyses. The work was supported by NIH grants R01 GM108043 to DLS and S10 RR027990 to TAN, and by funding from the European Research Council (grant agreement No. 637372) and the Independent Research Fund Denmark (grant agreement No. DFF-8021-00161) to BPP.

Methods

Expression of KdpFABC complex

For studies of serine phosphorylation, the pSD107 plasmid was transformed into E. coli strain TK2499 (both from W. Epstein, Univ. of Chicago), which lacks all other K^+ transport systems with genotype F^-, thi, rha, lacZ, nagA, trkA405, trkD1, Δ(kdpFABC)5, Δ(ompT). This plasmid was originally derived from pBR322 and contained the kdpFABC operon along with its endogenous promoter and an 8x histidine tag at the C-terminus of kdpC. Cells were grown in 4 L flasks at 31°C in K0-medium (46 mM Na_2PO_4, 23 mM NaH_2PO_4, 25 mM $(NH_4)_2SO_4$, 0.4 mM $MgSO_4$, 6 μM $FeSO_4$, 1 mM sodium citrate, 0.2% glucose, 1μg/mL thiamine, 50 μg/mL carbenicillin) supplemented with additions of 10 μM KCL every 90 min after culture density reached an OD_{600} of ~0.1. Total culture volumes ranged between 4-9 L. Cells were harvested at an OD_{600} of ~0.3-0.4 by centrifugation at 3500g for 20 min; the resulting cell pellets were frozen at -80°C for storage. For K^+ shock experiments, the culture was divided into equal portions and 20 mM KCl was added from a 2M stock solution followed by further incubation for defined periods of time prior to harvest.

To generate site-specific Ala mutants, site-directed PCR mutagenesis was used to alter codons in the WT operon on the plasmid described above. These plasmids were transformed into E. coli strain TK2498 with genotype F^-, thi, rha, lacZ, nagA, trkA405, trkD1, kdpA-Q116R, Δ(ompT), also from W. Epstein. Unlike TK2499, this strain carries a chromosomal copy of kdpFABC with the Q116R mutation on kdpA, which lowers potassium affinity to ~6 mM and has been identified as kdp-42 or kdpA42 in previous publications (Epstein et al., 1978; Siebers and Altendorf, 1989). This tag-less copy served to maintain cell survival in the low K^+ conditions required to induce pump expression in cases where the alanine mutant complexes were inactive. For expression, cells were incubated overnight at 37°C in 10 mL K5-medium (K0-medium supplemented with 5 mM KCl). This culture was transferred to 500 mL K1-medium (K0-medium supplemented with 1 mM KCl) and incubated at 37°C for 8 h. The 500 mL cell culture was transferred again to 18 L K0.2-medium (K0-medium supplemented with 0.2 mM KCl) and incubated at 31°C to induce expression of kdpFABC. Cells were harvested at a culture density of OD_{600} = ~0.8 by centrifugation at 3500g for 20 min at 4°C and cell pellets were either frozen or used immediately for purification.

For studies of EP formation, the kdpFABC operon with the 8x histidine tag was cloned into the pBAD vector (Invitrogen, Carlsbad CA) and introduced into E. coli strain Top10 (Invitrogen). Cells were grown in 4L flasks at 37°C in LB media supplemented with 100 mg/mL ampicillin to an OD_{600} of 0.5. Expression was then induced by addition of 0.02% arabinose and the culture continued to grow at 37°C for 4 h. Cells were then harvested by centrifugation as above and frozen for storage. Total culture volumes were typically 2 L.

Purification of KdpFABC

For purification of the KdpFABC complex, cells were resuspended in 50 mM Tris pH 7.5, 1.2 M NaCl, 10 mM $MgCl_2$, 10% glycerol, protease inhibitor tablets (Roche, Basel Switzerland) and 1 mM DTT, and lysed with an Emulsiflex C3 high-pressure homogenizer (Avestin, Ottawa Canada). Whole cells and debris were removed by centrifugation for 15 min at 12,000g, and membranes were pelleted by centrifugation for 2.5 h at 90,140g. Membranes were solubilized by overnight incubation in 50 mM Tris pH 7.5, 600 mM NaCl, 10 mM $MgCl_2$, 10% glycerol, 1 mM TCEP and 1.2% n-decyl-β-maltoside (DM) at 4°C using 20 mL per gram of membrane. After

centrifugation for 30 min at 90,140g, the solution was loaded on a 5 mL Ni-NTA HiTrap chelating column (GE Healthcare, Chicago IL) that was equilibrated in Ni-NTA base buffer (50 mM Tris pH 7.5, 600 mM NaCl, 10 mM $MgCl_2$, 10% glycerol, 1 mM TCEP, and 0.15% DM) supplemented with 20 mM imidazole. The column was washed with 20 mL of this same buffer, followed by 20 mL of Ni-NTA base buffer supplemented with 50 mM imidazole. Stepwise 5 mL elutions (collected in 1.5 mL fractions) were then performed as the imidazole concentration was incremented in steps of 50 mM up to a final concentration of 300 mM imidazole. Alternatively, elution was done with a continuous gradient running from 50 - 500 mM imidazole. The fractions containing KdpFABC were pooled, concentrated to ~0.7 mL using a 100 kDa cut-off Amicon centrifugal filter (Sigma Aldrich, St. Louis MO) and introduced onto a Superdex 200 size exclusion column (GE Healthcare) pre-equilibrated with 25 mM Tris pH 7.5, 100 mM KCl, 10% glycerol, 1 mM TCEP, and 0.15% DM. For measurements of EP formation, the NaCl was substituted for KCl during this purification. Fractions were either stored for short periods (days) at 4°C or frozen in liquid nitrogen and stored at -80°C.

Quantification of serine phosphorylation

The Phospho-Tag™ phosphoprotein gel stain kit (ABP Biosciences, Beltsville MD) was used to evaluate levels of serine phosphorylation. Specifically, 20 μg of precipitated protein was resuspended in sodium dodecylsulfate (SDS) buffer and run on a 10% SDS-PAGE gel. After staining according to manufacturer's instructions, gels were imaged in a Chemidoc imaging system (BioRad, Hercules CA) using the epi-green illumination for Cy3 fluorescence. KdpB-S162A was used as a negative control and a normalization factor for band intensities.

Localization of the site of serine phosphorylation and estimation of stoichiometry were done by nano-liquid chromatography-tandem mass spectrometry (nano-LC-MS/MS). Slices from SDS gels were digested with 500 ng trypsin solution (10 ng/μL) (Promega, Madison WI) in 50 mM NH_4HCO_3 and incubated for 4 h at 37°C, followed by 500 ng GluC or AspN protease (Promega) overnight. Digestion was stopped with 10% formic acid and peptides extracted with 5% formic acid in 50% acetonitrile, followed by final extraction with acetonitrile. Combined peptide pools were concentrated to a small droplet by centrifugation under vacuum. The resulting peptides were desalted using a Stage Tip manually packed with Empora C18 High Performance Extraction Disks (3M) (Rappsilber et al., 2007). Desalted peptide pools were dried under vacuum to a small droplet, and finally reconstituted to 20 μL with 0.1% formic acid.

LC-MS/MS was performed with a ThermoEasy nLC 1000 ultra high-pressure UPLC system (ThermoFisher Scientific, Waltham MA) coupled online to a Q Exactive HF mass spectrometer with NanoFlex source (ThermoFisher Scientific). Analytical columns (25-30 cm long and 75 μm inner diameter with 8 μm spray needle) were packed in-house with ReproSil-Pur C18 AQ 3μm reversed-phase resin (Dr. Maisch GmbH, Ammerbuch-Entringen, Germany). The analytical column was placed in a column heater (Sonation GmbH, Biberach, Germany) regulated to a temperature of 45°C. The peptide pool was loaded onto the analytical column with buffer A (0.1% formic acid) at a maximum back-pressure of 300 bar; peptides were eluted with a 2-step gradient of 3% to 40% buffer B (100% ACN and 0.1% formic acid) over 40 min and 40% to 90% B over 5 min, at a flow rate of 250 nL/min over 60 min before direct infusion into the mass spectrometer. Mass spectrometric data were acquired using a data-dependent (DDA) top-15 method, dynamically choosing the most abundant, not-yet-sequenced precursor ions from the survey scans (300–1750 Th). Peptide fragmentation was performed via higher energy collisional dissociation with a target value of 10^6 ions. Precursors were isolated with a window of

1.6 Th, survey scans were acquired with a resolution of 120,000 at *m*/*z* 200 and HCD spectra with 15,000 at *m*/*z* 200.

Mass spectra were first processed with Proteome Discoverer 1.4 and then compared with a SwissProt Database with a Taxonomy filter for E coli (22,982 sequences) from 072014 using Mascot (Matrix Science, London,UK). Decoy protein sequences with a reversed order were included to estimate false discovery rates, which averaged ~1% at protein and peptide levels. Peptide spectral matches were further analyzed with Thermo Scientific Xcalibur software. Phosphoserine peptide ion intensities (within 5 ppm of calculated mass) were manually extracted, and intensity ratios of singly phosphorylated peptides relative to total (phosphorylated and nonphosphorylated) peptide intensities were calculated for each sample.

Activity Assays

ATPase rates of purified KdpFABC were measured with a coupled enzyme assay (Warren et al., 1974) with 5 μg of protein in a total volume of 0.5 mL at 25°C. The standard assay buffer was composed of 75 mM TES pH 7, 150 mM KCl, 7.5 mM $MgCl_2$, 9.6 U/mL lactate dehydrogenase, 9.6 U/mL pyruvate kinase, 2.4 mM ATP, 0.5 mM phosphoenol-pyruvate, 0.36 mM NADH, and 0.15% DM. Concentrations of KCl and ATP were varied for determination of K_M. Orthovanadate was prepared by adjusting the pH of a 200 mM solution of sodium othovanadate to 10 using NaOH, boiling until the yellow color cleared, cooling to room temperature, and repeating this cycle until the pH stabilized. Data from titrations with K^+, ATP and VO_4 were fit using Prism8 software (GraphPad Software, San Diego CA).

For measurement of K^+ transport, KdpFABC was reconstituted into proteoliposomes using the method of Levy et al. (Levy et al., 1992). Specifically, a thin film of lipid (3:1 weight ratio of E. coli polar extract and 1-palmitoyl-2-oleoyl-sn-glycero-3-phosphocholine (Avanti Polar Lipids, Alabaster AL) was prepared by evaporating a chloroform stock solution (25 mg/ml) with Ar followed by 2 h in a vacuum chamber. This dry film was resuspended in transport buffer (20 mM HEPES pH 7.2, 5 mM $MgSO_4$, 140 mM potassium sulfamate, 1 mM N-methyl-D-glucamine sulfamate) to make a 10 mg/mL lipid stock solution, which was subjected to five cycles of freezing and thawing using liquid N_2. The stock solution was then extruded 13 times through a 400 nm nucleopore filter (Whatman plc, Maidstone UK) to create homogenous, unilamellar liposomes. Proteoliposomes were made using a lipid:protein weight ratio of 20:1, with 1.25 mg liposomes, 62.5 μg of KdpFABC, and 375 μg Triton X-100 (Sigma Aldrich) in a total volume of 250 μL. This solution was stirred at room temperature for 30 min followed by addition of 7.5 mg BioBeads (BioRad) and a further 90 min incubation. Finally, 15 mg BioBeads were added before overnight incubation with stirring at 4°C. Reconstituted proteoliposomes were harvested and bath-sonicated 3 times for 10 sec each before use in the transport assay.

The transport assay was performed as described by Damjanovic et. al. (Damnjanovic et al., 2013) using the voltage-sensing dye DiSC3 (Anaspec, Fremont CA). The assay was done in 2 mL reaction volumes comprising 25 μL proteoliposomes diluted in transport buffer, followed by the addition of 1 μM DiSC3 from a 1 mM stock in DMSO. Electrogenic transport by inside-out KdpFABC molecules was initiated by addition of 2 mM ATP, and the subsequent drop in fluorescence was fit to an exponential curve in order to calculate initial rate of transport. The fluorescent signal was measured with a Fluoromax-4 spectrofluorimeter (Horiba Scientific, Piscataway NJ) with excitation at 650 nm (5 nm slit), and emission at 675 nm (5 nm slit).

For measurements of EP formation, aliquots of purified KdpFABC were diluted to 0.25 mg/ml in 50 mM HEPES pH 7.8, 2 mM $MgCl_2$, 0.15% DM and 10 mM of either KCl or NaCl. The reaction was started by addition of 100 μM [γ32P]-ATP and 200 ml aliquots containing 25 mg of protein and 2.7 μCi were taken at intervals of 0, 15, 30, 60, 120 sec and quenched with 300 ml of 35% ice cold trichloroacetic acid (TCA). For the pulse-chase experiments, samples were incubated for 15 sec at 4°C, an aliquot was recovered followed by addition of 10 mM ADP and 10 mM EDTA with additional aliquots taken various time intervals. After completing the assay, aliquots were centrifuged for 10 min at 14,000g and washed twice with either 5% ice-cold TCA (for filtration) or water (for SDS-PAGE). For filtration, pellets were resuspended in 500 mL 5% TCA, filtered with 0.22 mm MCE filters (MilliporeSigma, Burlington MA) and washed 3 times with 5% TCA. Radioactivity was then quantified with a scintillation counter. For SDS-PAGE, the pellets were resuspended 30 mL of 5 mM TRIS-phosphate pH 5.8, 6.7 M urea, 0.4 M DTT, 5% SDS, 0.014% bromophenol blue. The stacking gel contained 4% polyacrylamide, 65 mM TRIS-phosphate pH 5.5, 0.1 % SDS. The resolving gel contained 7.5% polyacrylamide, 65 mM TRIS-phosphate pH 6.5, 0.1 % SDS. The running buffer was 0.17 M MOPS pH 6 and 0.1% SDS. Gels were dried and exposed to a storage phosphor screen overnight which was then imaged with a Typhoon Trio+ (GE Healthcare). All samples were collected in triplicate.

MD Simulations

To set up the system for simulation, a bilayer containing 550 lipid molecules was constructed using CHARMM-GUI with a 4:1 ratio of 1-palmitoyl-2-oleoyl-sn-glycero-3-ethanolamine (POPE) and 1-palmitoyl-2-oleoyl-sn-glycero-3-phosphoglycerol (POPG). The published crystal structure for KdpFABC (PDB: 5MRW), including the bound K^+ ion, water molecule and protein subunits, was introduced in the bilayer with the help of the PPM server associated with the Orientations of Proteins in Membranes database (https://opm.phar.umich.edu/ppm_server). Finally, the system was hydrated with 75,000 water molecules with 150mM of salt (KCl) in this aqueous phase.

All-atom MD simulations were carried out using GROMACS (Abraham et al., 2015) version 2016.3 under periodic boundary conditions. We utilized the TIP3P water model with Lennard-Jones interactions on hydrogen atoms. Non-bonded neighbor list was limited by a cutoff of 12 Å and was updated every 10 steps. The van der Waals interactions were turned off between 10 to 12 Å. The particle mesh Ewald (PME) method was used to model electrostatic interactions. All systems were minimized using steepest descent algorithm for 5000 steps. For each system - phosphorylated (PHOS) and not phosphorylated (SER) - ten independent simulations were run starting with different initial velocities. For each simulation, the converged system was equilibrated for 5 ns with backbone restraints on the protein followed by a production run of 200 ns. The temperature of the system was maintained at 310K with the Nose-Hoover thermostat after an equilibration run, which was performed with the Berendsen thermostat. The pressure was maintained at 1 bar with the Parrinello-Rahman barostat with a semi-isotropic pressure coupling scheme. The Linear Constraint Solver (LINCS) algorithm was utilized to constrain all bonds carrying hydrogen. A 2 fs time step was used and trajectories were sampled every 20 ps. The data analysis was carried out using GROMACS and python scripts. Snapshots were rendered using Visual Molecular Dynamics (VMD) (Humphrey et al., 1996).

Covariance and Principal Components Analysis was performed for the protein backbone atoms after accounting for bulk translation and rotation of the molecule. A covariance matrix C was extracted from atomic fluctuations

$$\mathbf{C} = \langle (\mathbf{x}(t) - \langle \mathbf{x} \rangle)(\mathbf{x}(t) - \langle \mathbf{x} \rangle)^{T} \rangle \quad (1)$$

where **x** is a 3N-dimensional column vector describing the 3-dimensional coordinates of the N protein backbone atoms, and **x**(t) are the spatial coordinates at time t. The triangular brackets indicate an ensemble average. The 3Nx3N symmetric matrix C was then diagonalized by a coordinate transformation R

$$\mathbf{C} = \mathbf{R}\Lambda\mathbf{R}^{T} \quad (2)$$

$$\Lambda = \mathbf{R}^{T} C R \quad (3)$$

This orthogonal transformation converts C into a diagonal matrix Λ = diag(λ1, λ2, ...λ3N), which contains the eigenvalues λi of the covariance matrix C. The *i*th column of **R** contains the *i*th eigenvector **r**i with the corresponding eigenvalue λi. The global collective motions of the trajectory were then obtained by projecting the trajectory ensemble onto individual eigenvectors, to generate the principal components pi, i = (1,2,...N), by taking an internal product between the transpose of the eigenvector and the atomic fluctuation

$$pi(t) = \mathbf{r}i \cdot (\mathbf{x}(t) - \langle \mathbf{x} \rangle) \quad (4)$$

Each trajectory snapshot, thus projected on two different eigenvectors, yields one point on the point cloud distributions shown in Fig. 7.

Competing Interests

The authors have no competing or non-competing financial interests to disclose.

References

Abraham, M.J., Murtola, T., Schulz, R., Páll, S., Smith, J.C., Hess, B., and Lindahl, E. (2015). GROMACS: High performance molecular simulations through multi-level parallelism from laptops to supercomputers. SoftwareX *1--2*, 19 - 25, 10.1016/j.softx.2015.06.001.

Altendorf, K., Booth, I.R., Gralla, J., Greie, J.C., Rosenthal, A.Z., and Wood, J.M. (2009). Osmotic Stress. EcoSal Plus *3*, 10.1128/ecosalplus.5.4.5.

Ballal, A., Basu, B., and Apte, S.K. (2007). The Kdp-ATPase system and its regulation. J Biosci *32*, 559-568, 10.1007/s12038-007-0055-7.

Buurman, E.T., Kim, K.T., and Epstein, W. (1995). Genetic evidence for two sequentially occupied K^{+} binding sites in the Kdp transport ATPase. J Biol Chem *270*, 6678-6685, 10.1074/jbc.270.12.6678.

Cali, T., Brini, M., and Carafoli, E. (2017). Regulation of Cell Calcium and Role of Plasma Membrane Calcium ATPases. Int Rev Cell Mol Biol *332*, 259-296, 10.1016/bs.ircmb.2017.01.002.

Clausen, J.D., Bublitz, M., Arnou, B., Olesen, C., Andersen, J.P., Moller, J.V., and Nissen, P. (2016). Crystal Structure of the Vanadate-Inhibited Ca(2+)-ATPase. Structure *24*, 617-623, 10.1016/j.str.2016.02.018.

Cortay, J.C., Bleicher, F., Rieul, C., Reeves, H.C., and Cozzone, A.J. (1988). Nucleotide sequence and expression of the aceK gene coding for isocitrate dehydrogenase kinase/phosphatase in Escherichia coli. J Bacteriol *170*, 89-97, 10.1128/jb.170.1.89-97.1988.

Damnjanovic, B., and Apell, H.J. (2014a). KdpFABC reconstituted in Escherichia coli lipid vesicles: substrate dependence of the transport rate. Biochem *53*, 5674-5682, 10.1021/bi5008244.

Damnjanovic, B., and Apell, H.J. (2014b). Role of protons in the pump cycle of KdpFABC investigated by time-resolved kinetic experiments. Biochem *53*, 3218-3228, 10.1021/bi500336w.

Damnjanovic, B., Weber, A., Potschies, M., Greie, J.C., and Apell, H.J. (2013). Mechanistic analysis of the pump cycle of the KdpFABC P-type ATPase. Biochem *52*, 5563-5576, 10.1021/bi400729e.

Epstein, W. (2003). The roles and regulation of potassium in bacteria. Prog Nucleic Acid Res Mol Biol *75*, 293-320, 10.1016/s0079-6603(03)75008-9.

Epstein, W. (2015). The KdpD Sensor Kinase of Escherichia coli Responds to Several Distinct Signals To Turn on Expression of the Kdp Transport System. J Bacteriol *198*, 212-220, 10.1128/JB.00602-15.

Epstein, W., Whitelaw, V., and Hesse, J. (1978). A K+ transport ATPase in Escherichia coli. J Biol Chem *253*, 6666-6668.

Fendler, K., Drose, S., Altendorf, K., and Bamberg, E. (1996). Electrogenic K^+ transport by the Kdp-ATPase of *Escherichia coli*. Biochem *35*, 8009-8017, 10.1021/bi960175e.

Galperin, M.Y., Higdon, R., and Kolker, E. (2010). Interplay of heritage and habitat in the distribution of bacterial signal transduction systems. Mol Biosyst *6*, 721-728, 10.1039/b908047c.

Garty, H., and Karlish, S.J. (2005). Role of FXYD Proteins in Ion Transport. Annu Rev Physiol, 10.1146/annurev.physiol.68.040104.131852.

Goldshleger, R., Patchornik, G., Shimon, M.B., Tal, D.M., Post, R.L., and Karlish, S.J. (2001). Structural organization and energy transduction mechanism of Na+,K+-ATPase studied with transition metal-catalyzed oxidative cleavage. J Bioenerg Biomembr *33*, 387-399, 10.1023/a:1010615422932.

Haruta, M., Gray, W.M., and Sussman, M.R. (2015). Regulation of the plasma membrane proton pump (H(+)-ATPase) by phosphorylation. Curr Opin Plant Biol *28*, 68-75, 10.1016/j.pbi.2015.09.005.

Hiraizumi, M., Yamashita, K., Nishizawa, T., and Nureki, O. (2019). Cryo-EM structures capture the transport cycle of the P4-ATPase flippase. Science *365*, 1149-1155, 10.1126/science.aay3353.

Huang, C.S., Pedersen, B.P., and Stokes, D.L. (2017). Crystal structure of the potassium-importing KdpFABC membrane complex. Nature *546*, 681-685, 10.1038/nature22970.

Huang, Z., Marsiglia, W.M., Basu Roy, U., Rahimi, N., Ilghari, D., Wang, H., Chen, H., Gai, W., Blais, S., Neubert, T.A.*, et al.* (2016). Two FGF Receptor Kinase Molecules Act in Concert to Recruit and Transphosphorylate Phospholipase Cgamma. Mol Cell *61*, 98-110, 10.1016/j.molcel.2015.11.010.

Humphrey, W., Dalke, A., and Schulten, K. (1996). VMD: visual molecular dynamics. J Mol Graph *14*, 33-38, 27-38, 10.1016/0263-7855(96)00018-5.

Jacquot, A., Montigny, C., Hennrich, H., Barry, R., le Maire, M., Jaxel, C., Holthuis, J., Champeil, P., and Lenoir, G. (2012). Phosphatidylserine stimulation of Drs2p.Cdc50p lipid translocase dephosphorylation is controlled by phosphatidylinositol-4-phosphate. J Biol Chem *287*, 13249-13261, 10.1074/jbc.M111.313916.

Jung, K., and Altendorf, K. (2002). Towards an understanding of the molecular mechanisms of stimulus perception and signal transduction by the KdpD/KdpE system of Escherichia coli. J Mol Microbiol Biotechnol *4*, 223-228.

Jung, K., Fried, L., Behr, S., and Heermann, R. (2012). Histidine kinases and response regulators in networks. Curr Opin Microbiol *15*, 118-124, 10.1016/j.mib.2011.11.009.

Laermann, V., Cudic, E., Kipschull, K., Zimmann, P., and Altendorf, K. (2013). The sensor kinase KdpD of Escherichia coli senses external K+. Mol Microbiol *88*, 1194-1204, 10.1111/mmi.12251.

Lai, S., Safaei, J., and Pelech, S. (2016). Evolutionary Ancestry of Eukaryotic Protein Kinases and Choline Kinases. J Biol Chem *291*, 5199-5205, 10.1074/jbc.M115.691428.

Levy, D., Gulik, A., Bluzat, A., and Rigaud, J.-L. (1992). Reconstitution of the sarcoplasmic reticulum Ca^{++}-ATPase: mechanisms of membrane protein insertion into liposomes during reconstitution procedures involving detergents. Biochim Biophys Acta *1107*, 283-298, 10.1016/0005-2736(92)90415-i.

Moller, J.V., Olesen, C., Winther, A.M., and Nissen, P. (2010). The sarcoplasmic Ca^{2+}-ATPase: design of a perfect chemi-osmotic pump. Quarterly reviews of biophysics *43*, 501-566, 10.1017/S003358351000017X.

Palmgren, M.G., and Nissen, P. (2011). P-type ATPases. Annual review of biophysics *40*, 243-266, 10.1146/annurev.biophys.093008.131331.

Pedersen, B.P., Stokes, D.L., and Apell, H.J. (2019). The KdpFABC complex - K(+) transport against all odds. Mol Membr Biol *35*, 21-38, 10.1080/09687688.2019.1638977.

Pereira, S.F., Goss, L., and Dworkin, J. (2011). Eukaryote-like serine/threonine kinases and phosphatases in bacteria. Microbiol Mol Biol Rev *75*, 192-212, 10.1128/MMBR.00042-10.

Poon, W.W., Davis, D.E., Ha, H.T., Jonassen, T., Rather, P.N., and Clarke, C.F. (2000). Identification of Escherichia coli ubiB, a gene required for the first monooxygenase step in ubiquinone biosynthesis. J Bacteriol *182*, 5139-5146, 10.1128/jb.182.18.5139-5146.2000.

Primeau, J.O., Armanious, G.P., Fisher, M.E., and Young, H.S. (2018). The SarcoEndoplasmic Reticulum Calcium ATPase. Subcell Biochem *87*, 229-258, 10.1007/978-981-10-7757-9_8.

Rajagopalan, K., Dworkin, J., and Nagle, E. (2018). Identification and Biochemical Characterization of a Novel Protein Phosphatase 2C-Like Ser/Thr Phosphatase in Escherichia coli. J Bacteriol *200*, 10.1128/JB.00225-18.

Rappsilber, J., Mann, M., and Ishihama, Y. (2007). Protocol for micro-purification, enrichment, pre-fractionation and storage of peptides for proteomics using StageTips. Nat Protoc *2*, 1896-1906, 10.1038/nprot.2007.261.

Rhoads, D.B., Laimins, L., and Epstein, W. (1978). Functional organization of the kdp genes of *Escherichia coli* K-12. J Bacteriol *135*, 445-452.

Roe, A.J., McLaggan, D., O'Byrne, C.P., and Booth, I.R. (2000). Rapid inactivation of the Escherichia coli Kdp K+ uptake system by high potassium concentrations. Mol Microbiol *35*, 1235-1243, 10.1046/j.1365-2958.2000.01793.x.

Schramke, H., Tostevin, F., Heermann, R., Gerland, U., and Jung, K. (2016). A Dual-Sensing Receptor Confers Robust Cellular Homeostasis. Cell Rep *16*, 213-221, 10.1016/j.celrep.2016.05.081.

Siebers, A., and Altendorf, K. (1989). Characterization of the phosphorylated intermediate of the K^+-translocating Kdp-ATPase from Escherichia coli. J Biol Chem *264*, 5831-5838.

Sorensen, T.L., Moller, J.V., and Nissen, P. (2004). Phosphoryl transfer and calcium ion occlusion in the calcium pump. Science *304*, 1672-1675, 10.1126/science.1099366.

Stock, C., Hielkema, L., Tascon, I., Wunnicke, D., Oostergetel, G.T., Azkargorta, M., Paulino, C., and Hanelt, I. (2018). Cryo-EM structures of KdpFABC suggest a K(+) transport mechanism via two inter-subunit half-channels. Nat Commun *9*, 4971, 10.1038/s41467-018-07319-2.

Su, J., Gong, H., Lai, J., Main, A., and Lu, S. (2009). The potassium transporter Trk and external potassium modulate Salmonella enterica protein secretion and virulence. Infect Immun *77*, 667-675, 10.1128/IAI.01027-08.

Toustrup-Jensen, M., Hauge, M., and Vilsen, B. (2001). Mutational effects on conformational changes of the dephospho- and phospho-forms of the Na+,K+-ATPase. Biochem *40*, 5521-5532, 10.1021/bi002367m.

Trotschel, C., Albaum, S.P., and Poetsch, A. (2013). Proteome turnover in bacteria: current status for Corynebacterium glutamicum and related bacteria. Microb Biotechnol *6*, 708-719, 10.1111/1751-7915.12035.

Walderhaug, M.O., Polarek, J.W., Voelkner, P., Daniel, J.M., Hesse, J.E., Altendorf, K., and Epstein, W. (1992). KdpD and KdpE, proteins that control expression of the kdpABC operon, are members of the two-component sensor-effector class of regulators. J Bacteriol *174*, 2152-2159, 10.1128/jb.174.7.2152-2159.1992.

Warren, G.B., Toon, P.A., Birdsall, N.J., Lee, A.G., and Metcalfe, J.C. (1974). Reconstitution of a Calcium-Pump Using Defined Membrane Components. Proc Nat Acad Sci *71*, 622-626, DOI 10.1073/pnas.71.3.622.

Xu, C.F., Lu, Y., Ma, J., Mohammadi, M., and Neubert, T.A. (2005). Identification of phosphopeptides by MALDI Q-TOF MS in positive and negative ion modes after methyl esterification. Mol Cell Proteomics *4*, 809-818, 10.1074/mcp.T400019-MCP200.

Figure Legends

Figure 1. Survey of alanine substitution mutants reveals inhibition and serine phosphorylation of KdpB. (A) The Post-Albers scheme for the reaction cycle of P-type ATPases alternates between two major conformations denoted E1 and E2. The E1 state binds ATP and produces the high-energy aspartyl phosphoenzyme intermediate (E1~P), which remains reactive with ADP. A spontaneous transition produces the low-energy E2-P intermediate, which no longer reacts with ADP but instead undergoes hydrolysis to produce the E2 species. (B) Very low levels of ATPase activity were obtained from a series of Ala substitution mutants. (C) Mass spectrometry of these Ala mutants revealed high levels of phosphorylation of Ser162 on KdpB. (D) Treatment of several of these mutants with LPP to remove serine phosphorylation resulted in significant stimulation of ATPase activity, supporting the notion that serine phosphorylation is inhibitory.

Figure 2. K^+ shock of E. coli cultures leads to serine phosphorylation of KdpB and inhibition of ATPase activity. For these experiments, bacteria were cultured at low K^+ concentrations to induce expression of kdpFABC; thereafter, the culture was split and one half was subjected to 20 mM K^+ for varying periods of time. (A) A 20 min K^+ shock resulted in loss of ~40% of ATPase activity, which was fully recovered by LPP treatment. (B) Serine phosphorylation levels for samples from panel A determined by mass spectrometry were much higher after K^+ shock. (C) ATPase rates from additional individual experiments with varying periods of K^+ shock. The time periods are nominal because harvest of cells required a 20 min centrifugation in their respective media. (D) Serine phosphorylation levels for samples in panel C determined by Phos-tag staining of SDS gels show an increase in serine phosphorylation levels that is proportional to the observed inhibition of ATPase activity. (E) ATPase activities from a single culture split into 4 batches and treated with K^+ for variable times show a graded inhibitory response. (F) Levels of serine phosphorylation for the cultures in panel E were determined by Phos-tag staining. (G) Data from all experiments were combined and show a reasonable correlation (R=0.56) between ATPase activity and levels of serine phosphorylation determined by mass spectrometry. The right-hand axis represents recalibration of the mass spectroscopy signal based on extrapolation of the fitted line. (H) Correlation of ATPase activities from all the experiments with levels of serine phosphorylation determined by Phos-tag staining produces a much better correlation (R=0.97). (I) Correlation of serine phosphorylation levels from mass spectrometry and Phos-tag staining.

Figure 3. Substrate affinities are not affected by serine phosphorylation. (A) K^+-dependence of the KdpA-Q116R construct expressed under control of the pBAD promoter was unaffected by LPP treatment (K_M = 8.6 and 10.9 mM for control and LPP treated samples, respectively), though V_{max} increased ~4-fold (1.2 to 5.0 μmoles/mg/min). (B) The ATP dependence of this KdpA-Q116R construct was similarly unaffected with K_M = 123 and 118 mM and V_{max} = 1.41 and 5.17 μmoles/mg/min for control and treated samples respectively. (C) The WT construct expressed at low K^+ concentrations under the native promoter was subjected to K^+ shock, thus inducing serine phosphorylation and a 40% decrease in ATPase activity. However, the inhibition of ATPase activity by vanadate was unaffected by the presence of serine phosphorylation (IC_{50} = 29.9 and 34.7 μM and V_{max} = 11.6 and 7.14 μmoles/mg/min, respectively).

Fig. 4. Steady-state levels of aspartyl phosphate (EP). (A-B) Individual experiments comparing time-dependence of EP formation at room temperature of several different constructs

in the absence (A) or presence (B) of 10 mM K^+. EP formation was initiated by addition of [γ^{32}-P]-ATP and aliquots were taken at various time intervals and quenched with TCA. The constructs are indicated in the legend. (C) Aggregated data from 15 individual experiments that have been normalized relative to levels for the E161Q construct. (D) Pulse-chase experiment in which samples have been incubated for 15 s with [γ^{32}-P]-ATP at 4°C to achieve maximal levels of EP (point at time zero) followed by addition of 10 mM ADP and 10 mM EDTA for the indicated time periods. As indicated in Suppl. Table 1, most of these constructs were double or triple mutants on the Q116R background as follows: Q116R = KdpA-Q116R. S162D = KdpA-Q116R/KdpB-S162D. S162A = KdpA-Q116R/KdpB-S162A. D307A = KdpA-Q116R/KdpB-D307A. E161Q = KdpA-Q116R/KdpB-S162A/KdpB-E161Q.

Figure 5. Water accessibility of the canonical ion binding site in KdpB. (A) Radial distribution functions between water molecules and the center of mass for Pro264, Thr265, Asp583 and Lys586 from KdpB, which surround the canonical ion binding site. The radial distribution function corresponds to a normalized histogram of distances between two atom selections, averaged over the time of the simulation. (B) Initial configuration of the canonical site for both the SER and PHOS simulations with a water molecule (blue) bound at the canonical ion binding site as seen in the X-ray structure. (C) and (D) Final frames from PHOS and SER simulations respectively. The canonical ion-binding site is significantly more hydrated in the PHOS simulations with water penetrating the site from the cytoplasmic side of the membrane (top of the panel).

Figure 6. Movement of cytoplasmic domains during the simulations. (A-C) Distributions of root mean square deviations for the three cytoplasmic domains, A, N, and P during the PHOS (blue) and SER (orange) simulations. All three domains are more mobile for the PHOS simulations compared to the SER simulations.

Figure 7. Principle component analysis of conformations sampled during the simulations. (A) Projection of individual frames from the simulation onto the first two eigenvectors (PC1 and PC2) from the covariance matrix. The prevalent conformation represented by the cloud labeled B is sampled by both PHOS and SER simulations. However, the PHOS simulation has sampled novel conformations represented by the peripheral clouds labeled C and D. Projections onto each individual axis are shown along as histograms along the top and right margins. (B-D) Structures extracted by k-means analysis of panel A from clouds B, C and D, respectively. Cytoplasmic domains are colored as follows: A-domain yellow, N-domain red, P-domain blue; transmembrane helices are grey.

Figure 8. Interactions between M1 and M2 helices control access of water to the canonical ion binding site. (A) Snapshot from the SER simulations shows the proximity of Glu87 on M1 and Arg212 on M2. The canonical binding site is below with relevant side chains shown as sticks. No water pathway is present. (B) Snapshot from the PHOS simulations shows that Glu87 and Arg212 are displaced and a water pathway is detected by CAVER (green surface) that leads to the canonical binding site. (C) Radial distribution function for center of masses from side chains of Glu87 and Arg212. Higher peaks for SER simulations indicate persistent interactions between these residues, whereas the lower peaks for PHOS simulations indicate that these interactions become disrupted. (D) Helical content of the linker between M2 and the A-domain (residues 68-92) is significantly lower for the PHOS simulations indicating unwinding of this structural element.

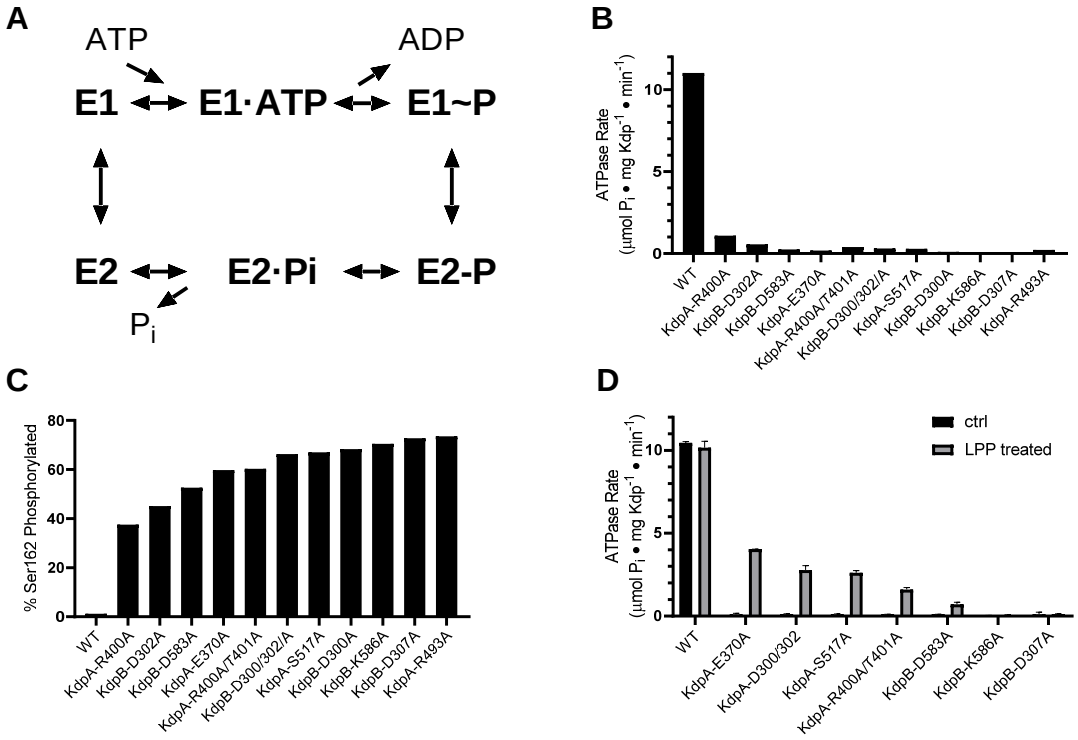

Figure 1

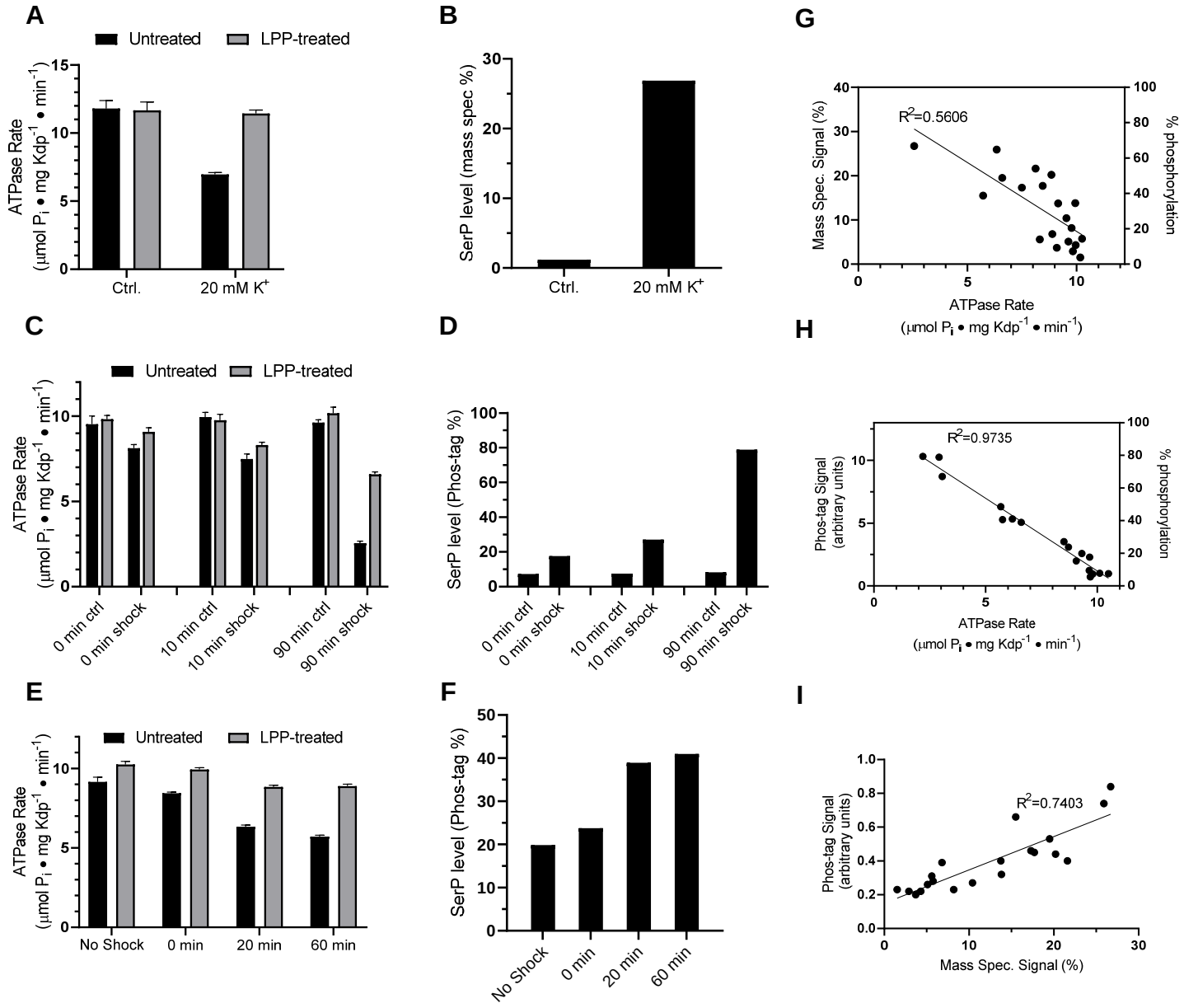

Figure 2

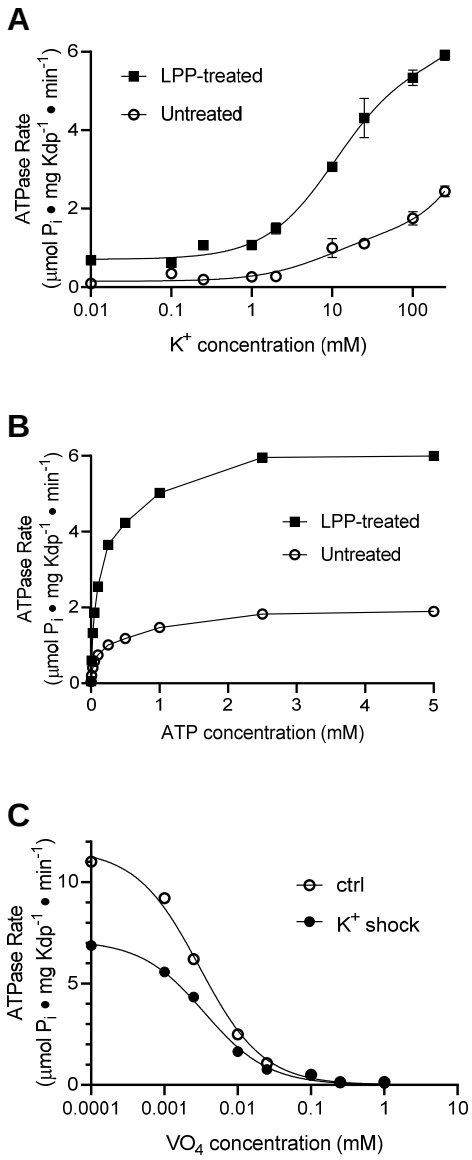

Figure 3

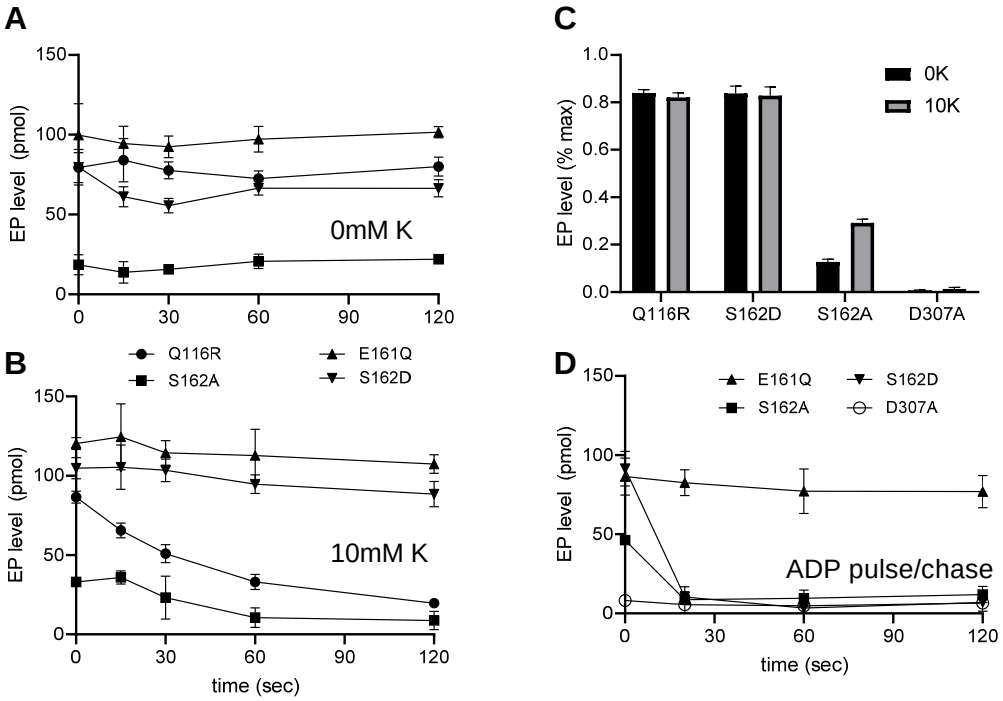

Figure 4

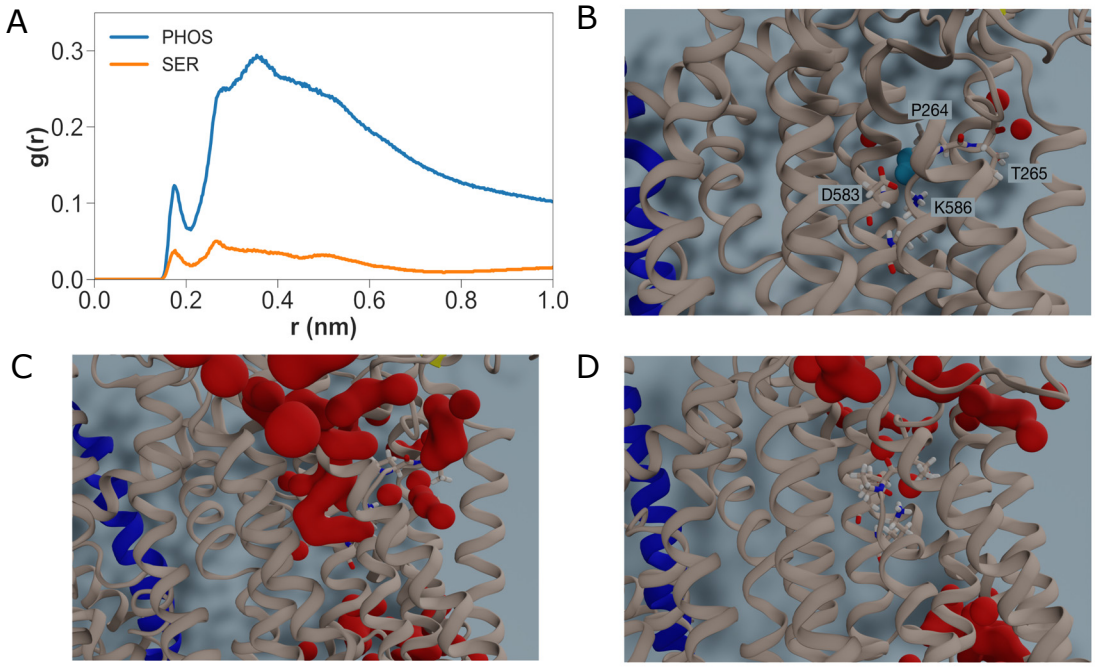

Figure 5

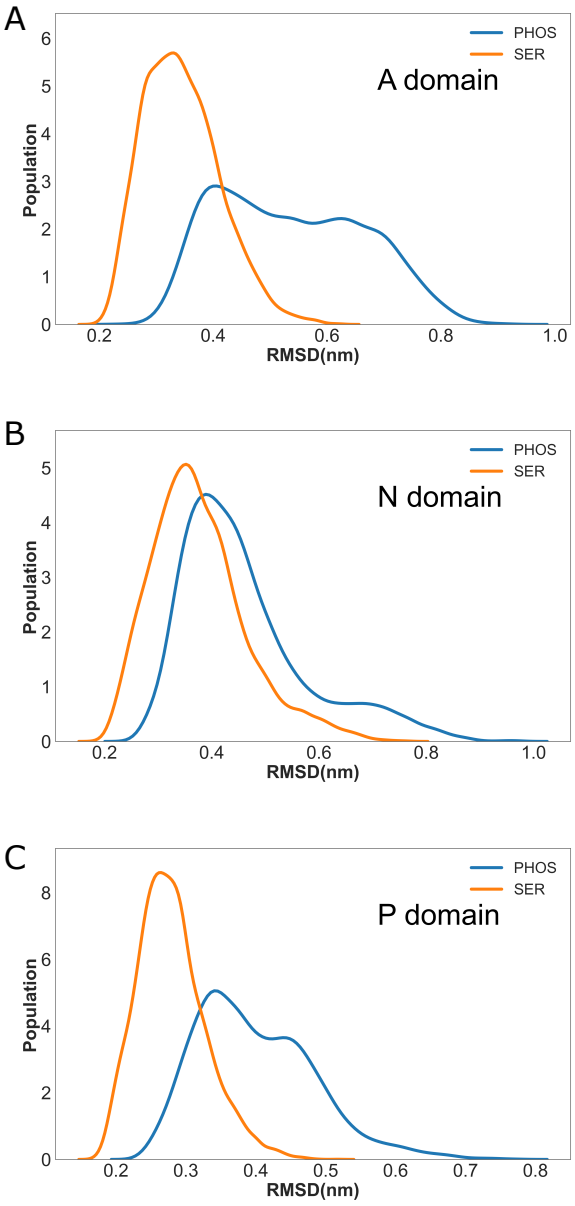

Figure 6

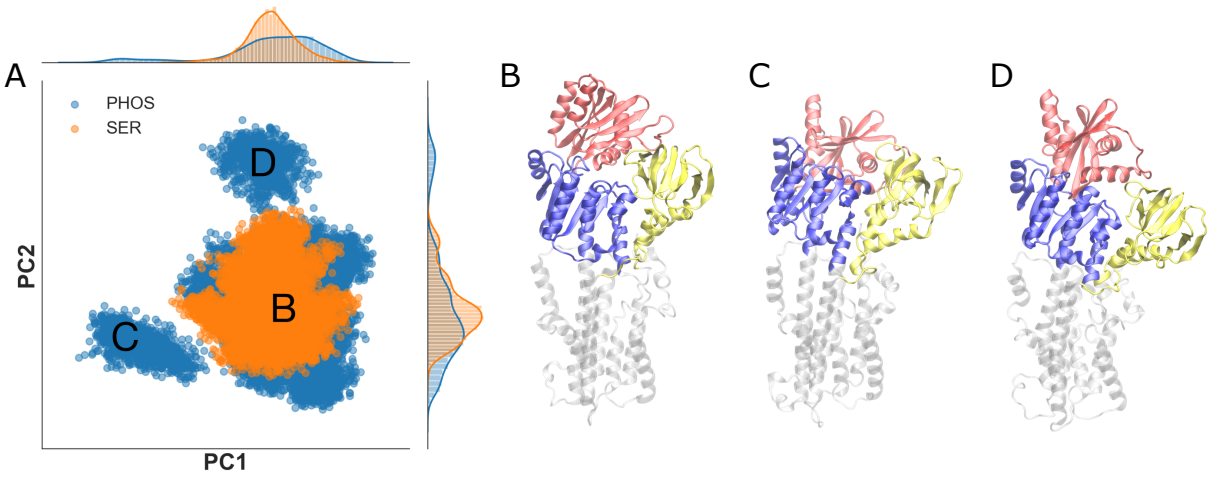

Figure 7

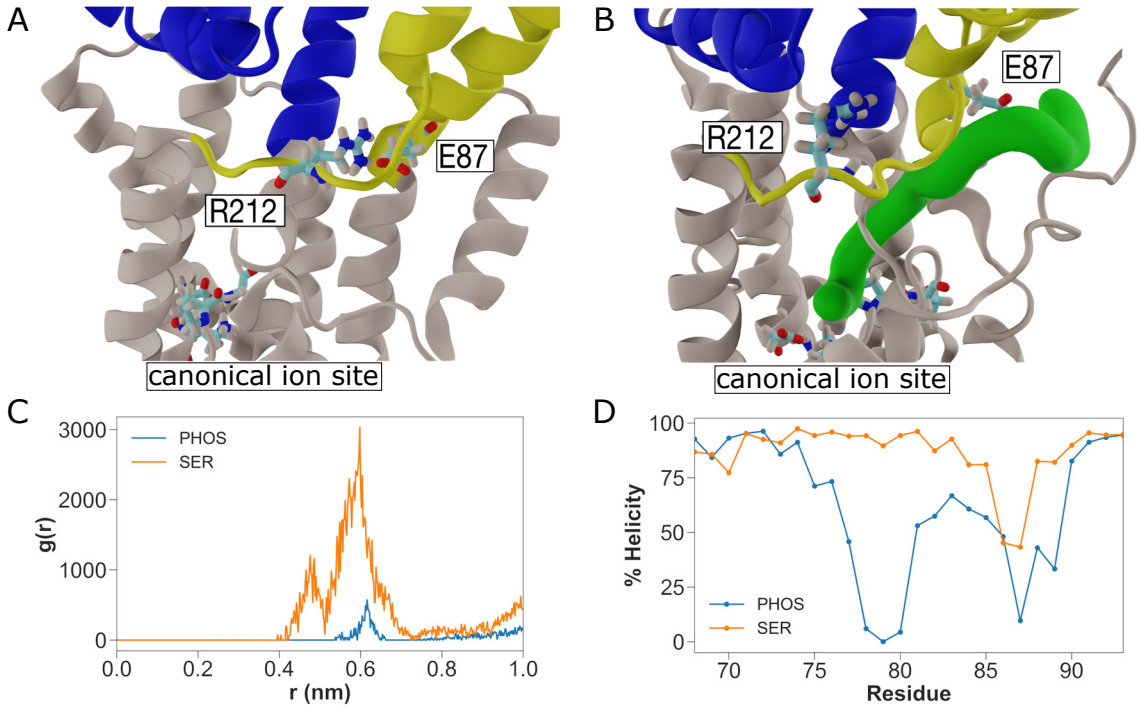

Figure 8